Liquid Crystals
Publication details, including instructions for authors and subscription information:
http://www.informaworld.com/smpp/title~content=t713926090

Static and dynamic textures obtained under an electric field in the neighbourhood of the winding transition of a strongly confined cholesteric

J. M. Gilli[a]; L. Gil[b]
[a] CNRS, INLN UMR 129 and URA 190, Faculté des Sciences de Nice, Nice, Cedex 2, France [b] CNRS, INLN UMR 129, Faculté des Sciences de Nice, France

To cite this Article Gilli, J. M. and Gil, L.(1994) 'Static and dynamic textures obtained under an electric field in the neighbourhood of the winding transition of a strongly confined cholesteric', Liquid Crystals, 17: 1, 1 — 15
To link to this Article: DOI: 10.1080/02678299408036545
URL: http://dx.doi.org/10.1080/02678299408036545

LIQUID CRYSTALS, 1994, VOL. 17, NO. 1, 1–15

Static and dynamic textures obtained under an electric field in the neighbourhood of the winding transition of a strongly confined cholesteric

by J. M. GILLI*
CNRS, INLN UMR 129 and URA 190,
Faculté des Sciences de Nice, 06108, Nice, Cedex 2, France

and L. GIL
CNRS, INLN UMR 129,
Faculté des Sciences de Nice, 06108, Nice, Cedex 2, France

(*Received 30 July 1993; accepted 1 November 1993*)

In recent work, Oswald and collaborators describe the thermodynamical phase diagrams of a large pitch cholesteric, confined between glass plates with homeotropic alignment conditions, in the neighbourhood of the critical confinement and in the presence of an AC electric field. In the case of a negative dielectric anisotropy, and with a low confinement ratio C, they have shown both experimentally and theoretically that the electrical destabilization possesses a second order character, as in the case of the nematic Fréedericksz transition. It is consequently possible to describe and to simulate numerically the equilibrium (under an AC field) and dissipative, out of equilibrium (under a DC field) patterns obtained experimentally, by the use of a Ginzburg–Landau model, deduced from symmetry arguments. The order parameter used here is the projection of the director in the mid-plane of the sample. The spiral shaped textures obtained in the out of equilibrium case are probably among the first simple physical analogues to the chemical and biological phenomena observed in the area of excitable media.

1. Introduction

The 2D dynamic patterns of the Belousov–Zhabotinsky reaction have found considerable interest in recent years in the area of out of equilibrium dissipative systems. Theoretical approaches, involving Ginzburg–Landau–de Gennes (G–L–dG) dynamical normal forms [1], have been developed and relations with Life Sciences and excitability have been proposed [2, 3].

These G–L models have been used less in the area of thermotropic liquid crystal (TLC) dynamics. Our recent work [4], concerning the bend Fréedericksz transition in the presence of a rotating magnetic field in the plane of the homeotropically anchored slab, demonstrates the efficiency of such an approach, and its ability to predict, in its greatest part, the formation, transformations, and time dependent behaviours of the continuous walls nucleated in the intensity/frequency phase diagram. In this case, it has been possible to derive directly a G–L–dG normal form from the Frank elastic energy density expression [4].

* Author for correspondence.

0267–8292/94 $10·00

This kind of normal form involves a complex order parameter and seems at first to limit its appliability to 2D problems with an in-plane vectorial order parameter, but our previous work [4] on nematic TLC materials, homeotropically anchored between parallel glass plates, shows that the projection of the mid-plane director **n** on the plane of the slab provides a useful complex order parameter to characterize transitions from a homeotropic unperturbed state to a more complicated situation in which the director comes out weakly from its initial perpendicular orientation to the glass plates. The weakness of the perturbation is necessary for the validity of the derived model.

Concerning now the experimental phenomena observed in regard to transitions of 'homeotropic-confined chiral organizations', the situations encountered obviously do not all fully correspond to this requirement of a low destabilization angle: the transition to the well-known 'Press–Arrot' (P–A) fingers [5], have had a first order character demonstrated in experimental studies made on positive dielectric anisotropy materials possessing, as is generally the case, a rather high elastic anisotropy [6].

But the recent work of Oswald *et al.* [7], demonstrates, both experimentally and theoretically, that it is possible to reach a second order behaviour in the case of negative dielectric anisotropy materials. There, as seen in the following, the static and dynamic G–L–dG approaches fully apply [8], and allow the description of the thermodynamical as well as the dissipative behaviours as propagative patterns of the P–A fingers, in the form of Archimedian spirals, rotating around topological defects. In this case, the more complex elasticity of chiral nematics does not at present allow us to derive directly the G–L–dG normal form which is here obtained from symmetry arguments. One interest in this approach lies in the complexity of the electric phenomena involved in the driving DC field used in this study. The model adopted here mainly requires a knowledge of the symmetries of this driving or forcing, and not an accurate physical description of these electrical effects involving possibly not only the simple quadrupolar coupling of **n** with a well-defined electric field perpendicular to the plate, but also inhomogeneous piezoelectric, space charge, and convective effects.

In the particular case of the 'mixed TLC' system used in the following, another problem arises from the possible coupling between the complex order parameter used and local concentration variations of the chiral dopant, associated with inhomogeneous orientational structures. As discussed elsewhere [9], the effect of this coupling probably consists mainly in the enlarged temperature domain of observability of these structures (and not to symmetry changes), relative to experiments made on pure materials.

2. Experimental set-up

The qualitative results described in the following have been obtained with two different nematic liquid crystals with a low content of chiral dopant. Both compounds possess a negative dielectric anisotropy and form the nematic phase at room temperature.

In order to reproduce the phase diagram of [7], the first system was the ZLI 2806 (E. Merck) mixture used in that previous work.

The second compound was the well-known MBBA, also used in the rotating-field Fréedericksz transition experiment of [4]. This material possesses a higher anisotropy of the magnetic susceptibility than ZLI 2806. This last fact is of great importance for extending the experiments of [4] to large-pitch cholesterics.

We used two different chiral dopants.

The first one was the Merck compound S811, as used in [1]. In this study, the ITO treated, conducting glass plates used (in order to apply a perpendicular electric field)

were coated with 1 per cent (w/w) lecithin/chloroform solution to obtain a homeotropic anchoring.

The second dopant used (SB) is a side-chain co-oligomer, described in [10] and furnished by Wacker Chemie. This particular molecule has a strong effect on the anchoring properties of the mixture, this probably being related to the affinity of the siloxane ring of SB for the coated glass plate; even at the very low concentrations used here, this molecule naturally induces a homeotropic anchoring, rendering the lecithin treatment superfluous.

The observations were made using an Olympus polarizing microscope, either at room temperature or employing a Mettler hot stage in order to increase the temperature and to speed up the pattern dynamics.

The static and dynamic patterns described below were obtained in the same voltage/confinement ratio regions of the phase diagram [7], and these observations were made for a large selection of sample thicknesses, d.

Our first trials were made with concentrations of chiral dopant close to 1 per cent (w/w). In this case, we had to work with rather low d ($\approx \mu$m), to reach a confinement ratio $C = d/P \leq 0{\cdot}7$ (where P is the natural pitch of the cholesteric) in order to make the director destabilization second order. Not having a cell that allowed continuous thickness (d) variations, we reproduced the same patterns with less concentrated solutions.

With chiral dopant concentrations of less than 0·2 per cent (w/w), it was possible to obtain the same behaviour as for d changing from 10 to 50 μm. In this case, the sample thickness, d, was known with better precision through the use of calibrated mylar spacers between the glass plates. The case of large d ($\approx 50\ \mu$m) is of particular interest for investigating, in the future, the effect of superimposing a magnetic field parallel to the plate.

3. Experimental results

3.1. *Quasi-thermodynamic equilibrium patterns with* $C < 0{\cdot}5$

As seen in the work described in [7] and on the left part of the phase diagram of figure 1, a homogeneous 'transitionally invariant cholesteric' (TIC) is directly obtained when the AC high frequency (1000 Hz) voltage V is applied between the glass plates. This transition, between the non-perturbed homeotropic texture, which appears black between crossed polarizers, and the TIC, is second order, and is induced for a particular voltage threshold $V_T(C)$. In fact, this phenomenon is very similar to the well-known Fréedericksz transition (FT) obtained for nematic TLC [4], under the same experimental conditions, corresponding, in figure 1, to the $C = 0$ domain. In particular, the complete tilt direction degeneracy of the director **n**, in the mid-plane of the sample, gives rise to the same kind of association of $+ -1$ disclinations patterns easily seen using the polarizing microscope (see figure 2 (*a*)). These disclination patterns slowly disappear with time through the progressive recombination of the $+1$ and -1 defects and do not constitute, strictly speaking, a thermodynamically stable state. The textures obtained in the chiral case show several important differences from the FT case.

When C is increased from its initial 0 value, V_T is slowly decreased from the theoretical Fréedericksz threshold $V = \pi\sqrt{K_3/\varepsilon_a} \approx 3{\cdot}5\ V_{eff}$ for MBBA, where K_3 is the bend elastic constant and ε_a the dielectric anisotropy of the TLC. This decrease can be easily understood if we remember that the chirality introduced has an influence opposed to the effect of the homeotropic anchoring, and 'helps' the electric field in its destabilizing role.

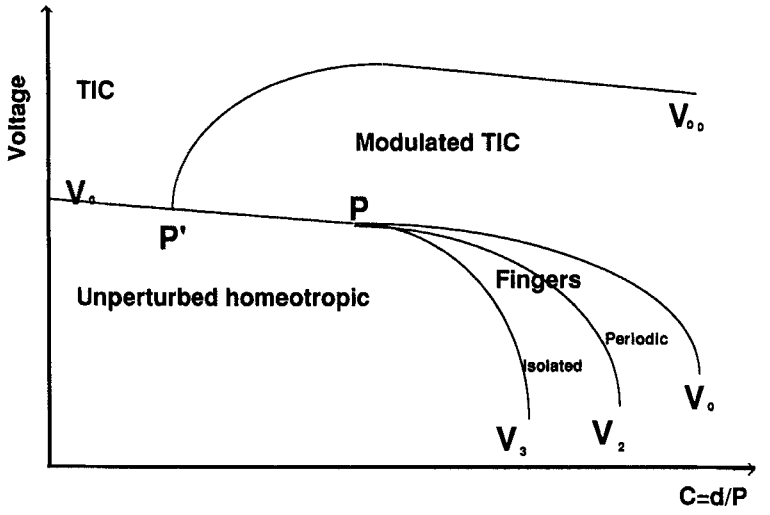

Figure 1. The thermodynamical phase diagram of voltage versus confinement ratio C for homeotropically anchored, chiral nematics, of negative dielectric anisotropy, as seen in [7].

In the pure FT, the four extinction lines, observed between crossed polarizers around the + − 1 vortex, correspond to a tilt direction of **n**, parallel or perpendicular to the polarizers, and this direction is the same when crossing the sample along the perpendicular to the plates, z. When C increases, these dark lines are no longer true extinctions because of the helical distribution of the tilt along z, and it is now necessary to rotate the analyser several tens of degrees from the initial crossed position to correct for the rotatory power of the slab and to obtain black lines.

We focus our attention now on the non-singular defects from which the lines start. Concerning the + 1 defects (easily distinguished from the − 1 defects by their rounded shape and by the behaviour of the dark lines when the polarizers are rotated), it appears now that they can be divided into two very different types (see figure 2 (*b*): (i) the first has a sharp core and the corresponding four dark lines are straight, (ii) the second presents a large homeotropic region in its core, easily detected in the neighbourhood of V_t. Moreover, this type is now associated with spiraling dark lines.

These two types of + 1 defects, both probably possessing a 'double-twist core', are respectively associated with the two different elastic energies of the two possible twisting senses of the core: the unfavourable twist is associated with the first type and a sharp core. This high-cost twist (opposed to the natural one induced by the chiral dopant) is restricted to a small region of space and we can identify the topology of this core with the one encountered in the centre part of the 'bubbles' recently discussed in [11]. The + 1 vortex with spiral lines is associated with the 'good twist' and possesses a favourable core. But the peripheral region of the defect needs now to spend some unfavourable in-plane bend elastic energy, as demonstrated by the spiral form of the lines: figure 3 shows that the topology of this second + 1 type is the analogue of the fingers loop described in [11]. As also seen in figure 3, it is clear that this second type can again appear with two different structures associated with the two possible spiral senses of the four lines (see figure 2 (*c*). In our preliminary experiments, the great majority of + 1 defects observed after application of a high voltage, belongs to the first type (see figure 2 (*d*). We observed some events corresponding to the transformation

of type 2 into type 1 defects, but never the reverse transformation. These last facts seem to correspond closely to the loop–bubble relations also described in [11].

Concerning now the -1 defects, the same asymmetry introduced with chirality is probably also responsible for a remarkable phenomenon: as V is increased, the -1 vortex elongates (see figures 2 (*a*)–(*d*) and progressively forms a lattice of homeotropic lines as seen in figure 2 (*d*). Each $+1$, of whatever type, is now at the centre of a cell limited by these walls. This phenomenon is understandable if we remember the topology of the -1 vortex; as seen in figure 4, both types of twist are present in the initial non chiral -1 defect, in the two orthogonal regions of the core. When chirality is introduced and the voltage increased, the favourable twist domain spreads out, and the unfavourable one becomes more and more constrained in a small region of space.

The pattern of the photograph constituted by a lattice of elongated -1 defects and an associated lattice of mainly, type 1, -1 defects, is in fact a complete topological analogue to the bubble domain mentioned for the first time in [12] in positive dielectric anisotropy materials. In the past, these bubbles were always obtained by 'out-of-equilibrium processes', such as strong voltage pulses or rapid cooling from the isotropic phase [11]: these 'out-of-equilibrium processes' correspond topologically to the one giving rise to the vortex field of the completely degenerate electric Fréedericksz transition.

3.2. *Thermodynamic equilibrium patterns with* $C > 0{\cdot}5$

As described in the literature [5–7], increasing the confinement ratio C leads to in homogeneous equilibrium structures (near the threshold of the voltage-induced destabilization), instead of the previously described TIC (see figures 1 and 2 (*a*)). The first one to appear, for $0{\cdot}5 < C < 0{\cdot}7$, is the modulated TIC, followed, when the tricritical point is reached ($C > 0{\cdot}7$), by the P–A fingers, these last being either isolated or associated in a periodic pattern.

As the tricritical point is approached, the asymmetrical fingers increase their width, and decrease their birefringence to a diffuse grey colour, related to a smaller and smaller destabilizing angle 2α [6] in the mid-plane of the sample, at the threshold of the electrically induced transition. Moreover, the transverse optical structure of the finger no longer shows the strong cylindrical-lens effect observed at higher C or for the positive dielectric anisotropy materials. In this case, the system undergoes a slightly sub-critical first order transition, and it can be assumed that α remains small. Another consequence of being in the tricritical point neighbourhood is that it becomes harder and harder to differentiate the isolated-finger domain from the periodic-finger domain.

3.3. *Spiral 'out-of-equilibrium' patterns in the presence of a DC electric field*

If we now apply, in this same 'quasi-second order' finger domain, close to the tricritical point, an increasing DC field, the nucleating low 2α angle fingers now take the shape of rotating Archimedian spirals as seen in figure 5 (*a*)–(*d*) These spiraling fingers preserve clearly the asymmetry of their tips, which strongly suggests an orientational structure very close to that of the Press–Arrot fingers. This is not the case for the Archimedian patterns previously observed at higher C, for an AC low frequency field and positive dielectric anisotropy materials [7 (a), 13]. As more accurately discussed in the theoretical part of this paper, these spirals generally develop around their normal tip, the sense of rotation being consequently fixed by the sense of the low amplitude, symmetry-breaking continuous field. Exceptions to this rule are observable (see figure 5 (*b*) in the case of a few multi-armed spirals, whose sense of rotation is

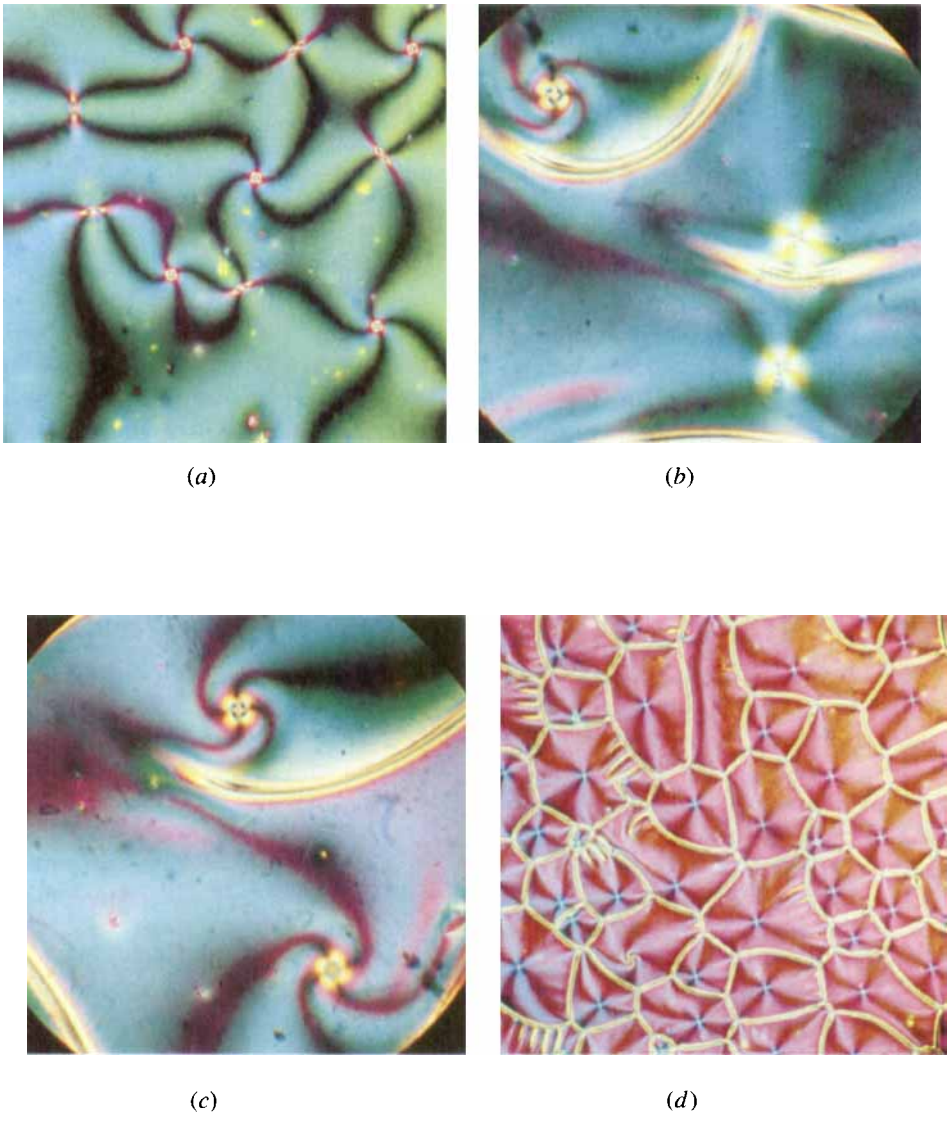

(*a*) (*b*)

(*c*) (*d*)

Figure 2. (*a*) An umbilical texture induced by the AC 1000 Hz electric field in the MBBA–S811 ($\approx 0{\cdot}2$ per cent w/w) mixture. The analyser has been rotated a few tens of degrees from the crossed position to correct for the rotatory power of the sample and to reobtain the extinction lines around the defects. The thickness d of the sample is 12 μm. The core of the + 1 umbilics have a rounded shape and the extinction lines starting from them have a spiral form. The − 1 umbilics clearly show an elongated shape. (*b*) At higher magnification than (*a*) and for a higher voltage, a favourable twist, large core, + 1 umbilicus with spiraling extinction lines is observed in the upper left corner. The two, yellow coloured, + 1 umbilics on the right are unfavourable twist, narrow core defects. Each + 1 umbilicus is associated with an elongated domain of − 1 topological charge. (*c*) In the same conditions as (*b*); the two equivalent, possible spiraling senses of the favourable twist, large core, + 1 umbilics are observed. (*d*) With the same enlargement as (*a*) and having applied abruptly an AC voltage of about 10 V_{eff}, the + 1 umbilics are now surrounded by a lattice of lines corresponding to the initial − 1 defects. Only one favourable twist core + 1, with spiral extinction lines, is observable in the bottom left corner.

(*a*)

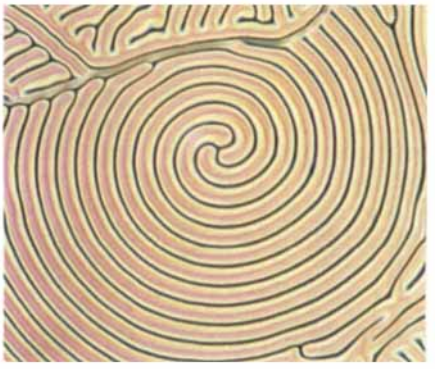

(*c*)

(*b*)

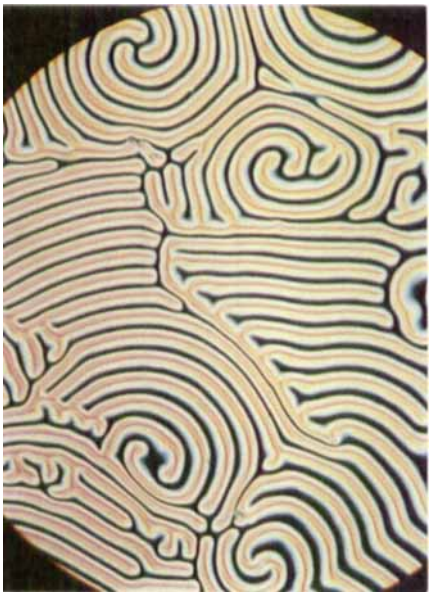

(*d*)

(i)

(ii)

Figure 5 (*caption overleaf*).

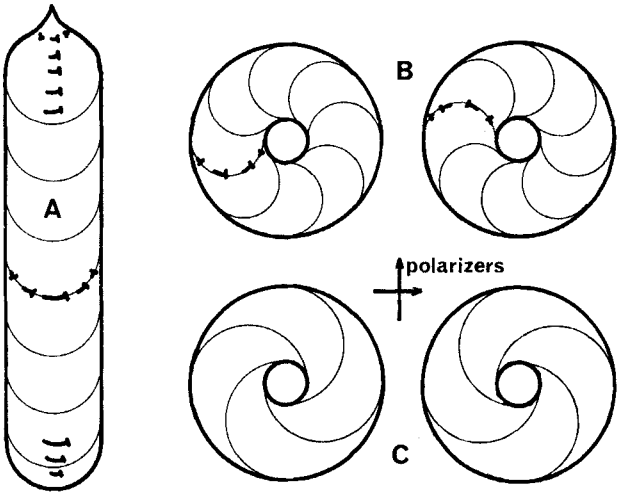

Figure 3. The orientation of the director is depicted using the nail convention. (*A*) The structure of the P–A fingers in the mid-plane of the sample. We assume here a right-handed chirality, corresponding to a left-handed favourable twist. A favourable in-plane twist is expressed in the peripheral region of the finger, except in the upper abnormal tip. As for (*B*), the thin lines represent the in-plane projection of the director lines of force. (*B*) The two possible topologies of loops obtained by both possible curvatures of the initial straight finger. (*C*) The thin lines now represent the locus in which the director projection is either parallel or perpendicular to the polarizer direction.

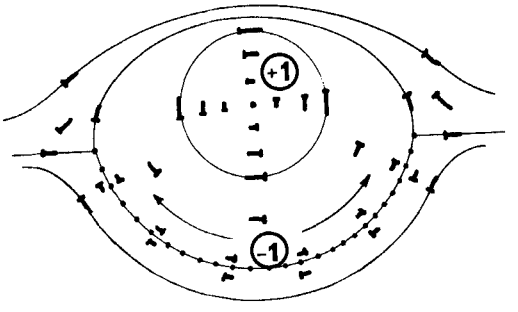

Figure 4. The topological association of an unfavourable twist core + 1 with an elongated − 1.

Figure 5. (*a*) Formation of P–A, dynamical, spiral shaped fingers, in a 12 μm thick sample in the presence of a 4 V DC field. The system is here very close to the triple point of the phase diagram in figure 1. Bubbles and + 1 defect 'two rounded end' fingers are also observable in the periphery of the spiral. (*b*) Same as (*a*) with lower thickness samples ($\approx 3\ \mu$m). Depending on the initial conditions, 1, 2 or 3 arm spirals can be obtained. Given the DC field sense, all the spirals have the same handedness. One exception to this rule is observed in the lower part of the photograph: in fact the double arm, reverse sense spiral is rotating around a + 1 umbilicus corresponding to the core of the bubbles. The centre of the normal spirals with rounded normal ends can be associated with a virtual − 1 defect. (*c*) Same as (*a*), closer to the tricritical point. The homeotropic regions are very thin between the spiraling fingers. A very regular spiral is formed. (*d*) (i) and (ii). The spirals change their handedness when the sense of the DC electric field is reversed. In these photographs, the sample was a few μm thick and the spirals were obtained by the application of a 1000 Hz 2·5 V_{eff} AC field, superimposed on a DC component of 1·5 V.

reversed relative to the single-arm kind: this is easily explained by the fact that the rotating centre of these multi-spirals is in fact constituted by the association of abnormal tips constituting a +1 defect with 'unfavourable twist core', comparable to the topology of the bubble domains.

One problem concerning these preliminary observations of Archimedian spiral waves in the presence of a DC field is related to the closeness of the onset of dynamical convective phenomena, also induced by the DC field. It is possible to avoid this problem completely and to observe more easily the spiral patterns by the use of an association of a high frequency AC field with a DC offset in a typical voltage ratio of 50/50. It is worth noting that it has not been possible to obtain the phenomena of P–A spiraling fingers by applying an AC field alone.

4. Theory

4.1. *The model*

As mentioned in §1 and more fully described in [8], we have recently derived a G–L–dG normal form equation describing this winding cholesteric transition.

The simplest complex order parameter one could use to describe the experiment would be the projection of the director **n** onto the mid-plane of the slab (i.e. $n_x + in_y$), but this is not invariant under the $n \rightarrow -n$ transformation. We consequently take as our order parameter the complex number $A = n_z(n_x + in_y)$, which is also a member of the projective sphere P^2.

Taking into account the invariances of the system under space rotation around the vertical z axis and the turn over of the sample, exchanging the upper and lower glass slides, and considering first the thermodynamical situations described by

$$\frac{\partial A}{\partial t} = -\frac{\partial F}{\partial \bar{A}},$$

where F stands for the real two-dimensional free energy density of the system [8], we get the following rescaled equation:

$$\frac{\partial A}{\partial t} = \mu A + A_{\chi\bar{\chi}} + \delta \bar{A}_{\chi\chi} + \mathrm{i}\eta(AA_{\bar{\chi}} + \bar{A}A_{\chi}) - |A|^2 A + \zeta F_4,$$

where $A_x = \partial A/\partial x$ and $\partial\chi = \partial x + i\partial y$. The fourth order F_4 term is necessary to define the lower boundary of the free energy: nine possible terms are allowed by the symmetry, but the results and simulations discussed in the following are not qualitatively changed by an arbitrary selection of a limited number of such terms.

The first term on the right controls the TIC stability and μ is proportional to $C - C_c$, where C_c is the critical confinement parameter: in the presence of an electrical field, it conveys also the quadrupolar coupling and is proportional to V_{eff}^2. The second term is a laplacian, invariant under a rotation around the z axis. It is analogous to the term with the L_1 elastic coefficient in the Landau–de Gennes free energy expression. In the isotropic elasticity case ($K_1 = K_2 = K_3$), it expresses the tendency of the director to keep the same orientation through all the sample. Both the third and fourth terms in the equation convey the anisotropy of elasticity of the liquid crystal. The fourth term, which is not invariant by the mirror symmetry, is proportional to the chirality $1/P$. The third term, associated with the elastic anisotropy, has already been derived in another experimental situation dealing with a nematic [4]. In our case, it seems to control the growth shape of the cholesteric (branching behaviour and shapes of finger tips). However, in this paper, we will not focus on these effects, and will neglect, in the

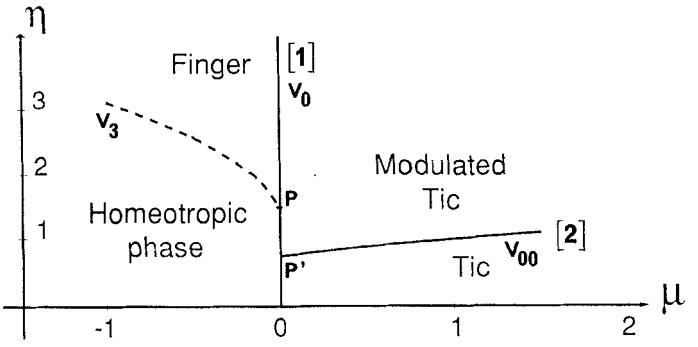

Figure 6. The time-independent phase diagram of the winding transition of the homeotropically anchored cholesteric, obtained from analytical (full lines) and numerical (dotted line) analysis of the G–L–dG normal form in the μ/η parameters space.

following, this third term, which vanishes in the classical 'one constant' approximation ($K_1 = K_2 = K_3$).

We now compare the solutions of the 'quasi-thermodynamic' equilibrium situation ($\partial A/\partial t \approx 0$) of our equation to the experimental and theoretical model of [7] and find the phase diagram of figure 6 in the μ/η parameter space. The full lines correspond to analytical analysis and correspond:

Line (1) to the absolute lost of stability of the trivial unperturbed homeotropic solution, $A = 0$ as μ increases. This line corresponds to the V_0 spinodal line of [7].

Line (2) to the appearance of a spatial perturbation of the homogeneous destabilized solution (the TIC-modulated TIC transition) and to the V_{00} line of [1]. The highest instability rate is obtained for a critical wavevector proportional to η.

The 'fingers solutions' appearance at sufficiently high η is confirmed numerically (see figure 7).

The dotted line separating the homeotropic nematic phase from the finger region corresponds to the spinodal line V_3 of [7] and to the absolute loss of stability of the regions of perturbed fingers. This line is obtained from a one-dimensional numerical analysis unadapted to take account of the energy difference between the regions of 'isolated fingers' and 'periodic fingers' separated by the line V_1 of [7]. Moreover, the critical line V_2 of [1] cannot be obtained from our model which does not take account of thermal fluctuations.

The intersections of the TIC-modulated TIC line (figure 6, line (2)) and of the numerical 'fingers line' (figure 6, line (1)) seem to correspond to the two triple points P and P' of [7]. The triple point P' is analytically obtained from the G–L–dG equation at the intersection of lines (1) and (2). The tricritical point P is obtained from a numerical analysis: even for a very accurate calculation of the V_3 dotted line, its intersection with line (1) remains separated from the P' point.

The metastability of the homeotropic and finger structures observed at the transition when crossing the dotted line seems to confirm its 'first order' character. The character of the line (1) in the region of the phase diagram where it separates the homeotropic domain from the TIC domain is unambiguously 'second order' as in [7]. The case of line (2) is less clear: as also observed experimentally, this transition is associated with

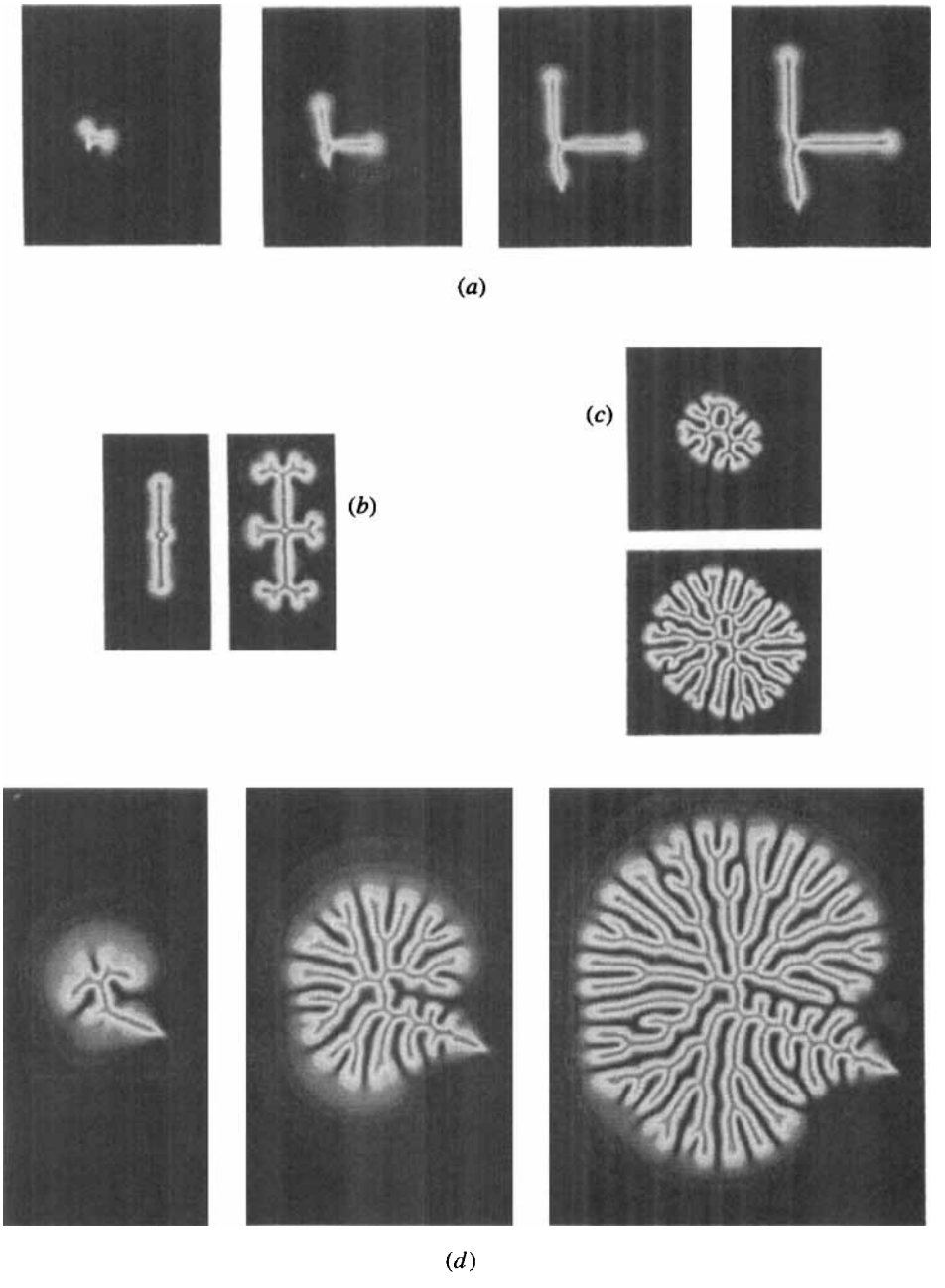

Figure 7. Simulations of the thermodynamical G–L–dG normal form in the slightly sub-critical P–A fingers domain. The white regions of the figures correspond to the occurrence of a non-zero modulus of the order parameter A. Different growth shapes of the fingers corresponding: (*a*), (*b*), (*c*) to $\mu = -0{\cdot}125$, $\eta = 2{\cdot}2$, (*a*) growth of an 'isolated finger' with two normal and one abnormal tip, illustrating the possible side-branching by recombination of the abnormal tips, (*b*) growth and branching of a 'two normal tips' finger starting from a $+1$ core bubble, (*c*) growth of a looped finger after recombination of the abnormal and normal tips, (*d*) to $\mu = 0{\cdot}1$ and the equilibrium structure is the modulated TIC. The growth is operated through the branching of normal and abnormal (on the right) tips.

a 'phase instability' which operates with particularly long delays, and the numerical analysis does not allow the determination of the transition order.

4.2. *The 2D simulations of the equation*

Figure 7 gives examples of finger growth obtained by simulation of the previous equation in the presence of random noise corresponding to thermally induced director fluctuations. The spatial variation of the A modulus is plotted here. The different shapes of fingers with normal and abnormal tips are easily observable.

Depending on the equation parameters, different dynamical behaviour is observed. In particular, the branching tendency, and growth speed of the two different tips can be obtained and will be described in detail in a future publication. The tendency of the abnormal tips to recombine perpendicular to the finger and to form finger-loop structures analogous to favourable core $+1$ disclinations can be obtained, as well as the variable density of spontaneously nucleated bubble domains of unfavourable twist core. The influence of the complete set of parameters, including the noise amplitude and the electric field distance from the destabilization threshold, can be studied in great detail in these 'simulation experiments' and compared to the 'true experiments' made on the chiral samples. As an example, figure 8 clearly reproduced the influence of the amount of chirality η, showing the previously discussed relation between the TIC $+ -1$ disclination pattern at low η and the bubbles-finger loops at high η. The proportionality of the wavevector to the chiral parameter is also illustrated in these same figures.

4.3. *The 'out-of-equilibrium' case*

We tackle now the out-of-equilibrium dynamics and the formation of the Archimedian shaped P–A fingers, experimentally obtained in the presence of a vertical DC electric field. In contrast to the microscopic interpretation of Hinov and Kukleva [14], who explain some of the spiral patterns they observed by possible gradient flexoelectric generation of point singularities, we adopt here a more general point of view, focusing on the generic way in which to perturb the previous G–L–dG equation. The thermodynamical description must be only slightly modified and our analysis could consequently be applied only to the case of 'weak electric field amplitudes'.

The new terms we look for have to be (i) invariant under the symmetry transformation used before and (ii) of as low an order as possible.

The turn-over symmetry transformation has to be modified because of the presence of the constant vertical electric field E_z ($\partial_x \to \partial_x, A \to -A, E_z \to -E_z$). The sign change of E_z is fundamental, since it leads, at first order in A, to complex coefficients.

The resulting perturbed equation is then

$$\frac{\partial A}{\partial t} = (\mu + \imath\nu_0 E_z)A + (1 + \imath\nu_1 E_z)A_{\chi\chi}^{-} + (\delta + \imath\nu_2 E_z)\overline{A_{\chi\chi}}$$

$$+ \imath\eta(AA_{\chi}^{-} + \bar{A}A_{\chi}) - |A|^2 A + \zeta(|A|^2 A_{\chi\chi}^{-} + \bar{A}A_{\chi}A_{\chi}^{-}).$$

Corrections to the real coefficients and to the non-linear terms are not taken into account, since E_z and A are supposed to be small.

Two-dimensional simulations of this last equation, starting from a thermodynamical finger structure and increasing ν_0, up to a weak non-vanishing value, reveal a transverse drift of the central part of the fingers (see figure 9). However, this drift is not uniform all along the finger, and, being slower near the rounded end, rolls the finger up around

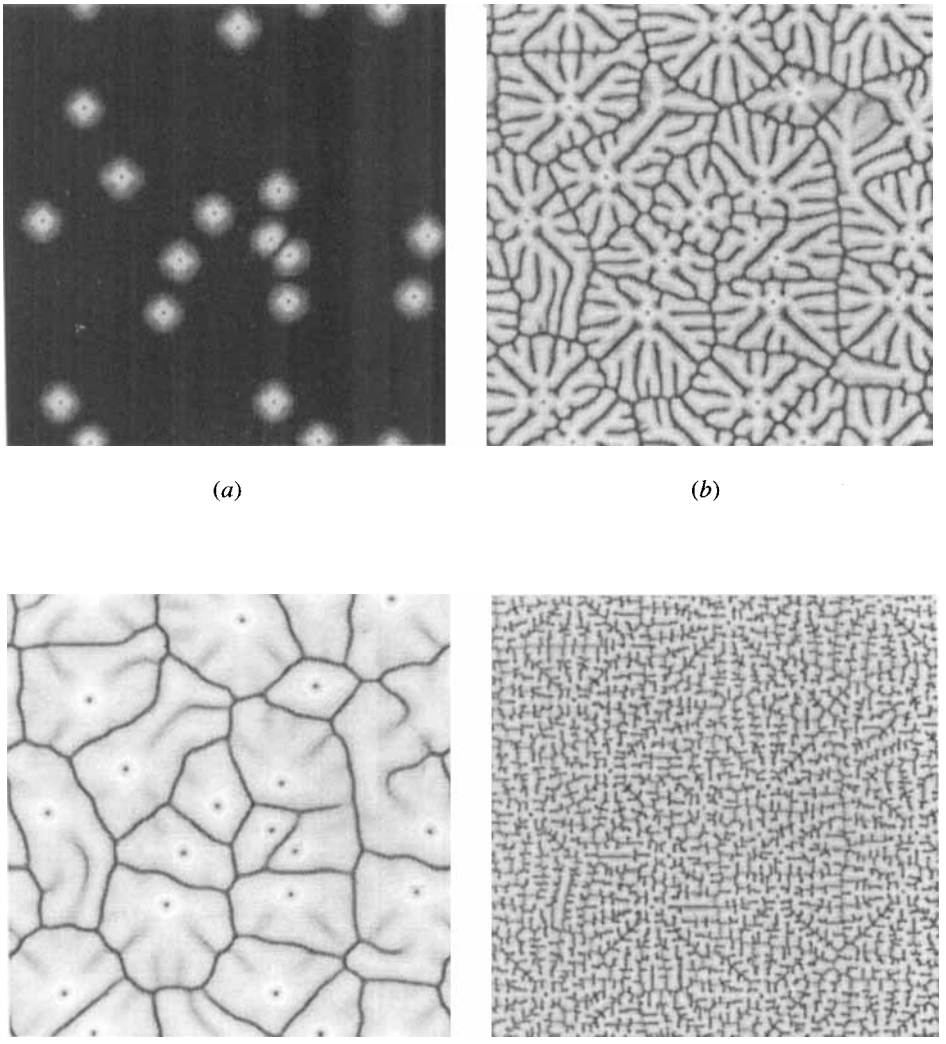

(*a*) (*b*)

(*c*) (*d*)

Figure 8. (*a*) $\eta = 2{\cdot}5$. The bubbles are (i) obtained by the application of a high pulse of μ starting from an initial condition of random noise and (ii) stabilized at $\mu = -0{\cdot}25$. (*b*), (*c*), (*d*) $\mu = 1$, we are now changing the chirality of the system and observe the η dependence of the modulation wave-vector; (*b*) $\eta = 2{\cdot}5$; (*c*) $\eta = 1$, and the pattern is very close to the experimental figure 2 (*d*); (*d*) $\eta = 5$.

its normal tip and forms an Archimedian spiral, in remarkable agreement with the experiment previously described: for a given sign of η and v_0, all spirals have the same handedness; this handedness is reversed when the sign of either of these two parameters is flipped.

The dynamical spirals patterns reported in [14] for samples of large thickness, also obtained in [7 (a) and 13], for an AC field with larger confinement ratios, are not treated by our model. The arm structure of these spirals corresponds probably to very large α angles, with trajectories of the director on the S^2 sphere passing close to the south pole.

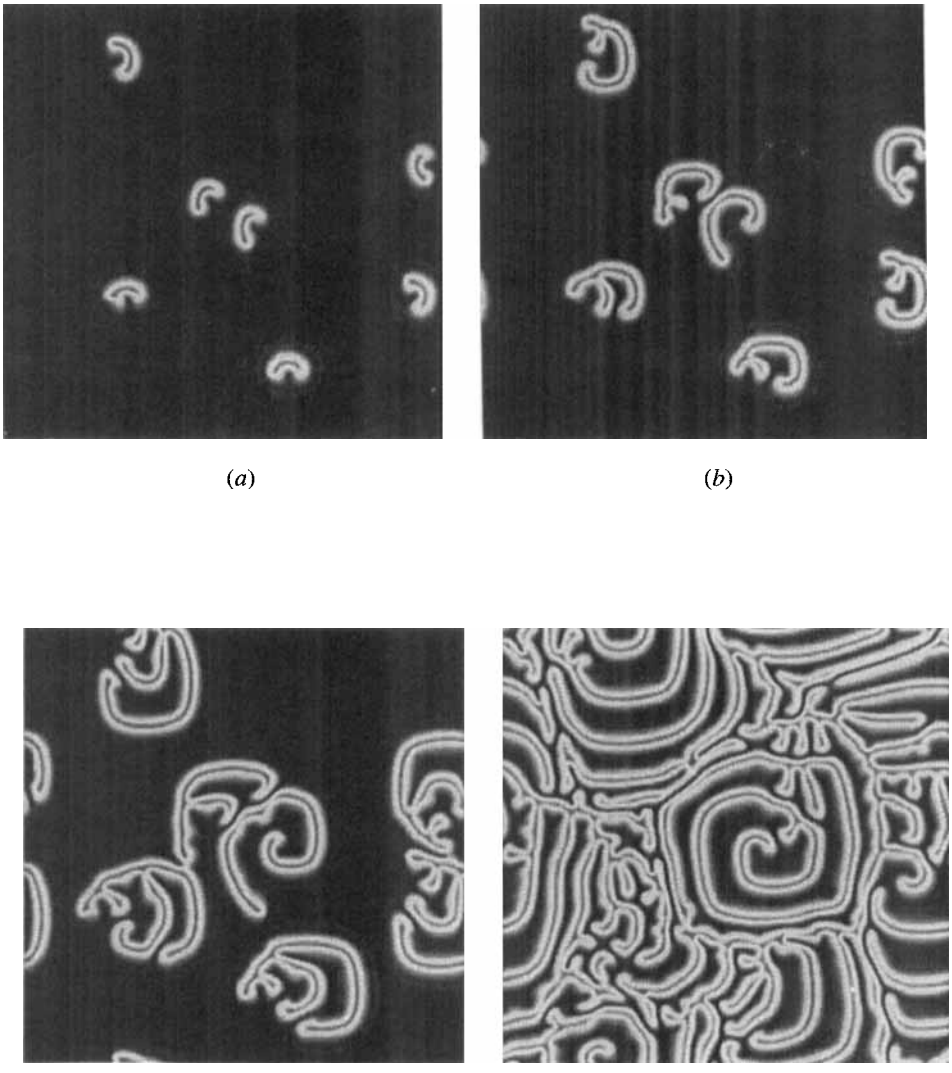

(*a*) (*b*)

(*c*) (*d*)

Figure 9. Simulation of the 'out-of-equilibrium' normal form $\mu = 0{\cdot}125$, $\eta = 2{\cdot}5$, and $\nu = 0{\cdot}2$: we observe the growth of fingers in the form of one-handed spirals rotating around their normal tip. The sign change of v_0 gives rise to a change of the handedness of the spirals.

As an aside, we want to underline the possible relevance of the low-destabilization-angle structures described above for data storage on erasable supports. The local degeneracy of the tilt (electrically induced) can be removed by the additional presence of a small magnetic field parallel to the sample plane. In this case, the tilt direction can be continuously varied all around the z axis for each memory element, thus allowing for high density storage. The tilt direction of each element can be easily detected by optical methods. These elements will have a typical lateral extension of the order of the thickness, d, of the liquid crystal slab ($\approx$ the size of the bubbles [11]) and their writing time will depend strongly on the rotational viscosity constant of the material

used and on the value of the applied destabilizing voltage. The use of a low molecular weight liquid crystal polymer having a glassy transition above room temperature, such as the one described in [10], also gives the opportunity of quenching such a tilt.

In conclusion, we have experimentally investigated the static behaviour and defect structures of a confined cholesteric slab for small values of the confinement parameter C, and a particular dynamical process, leading to the formation of dynamical patterns of Archimedian spirals in the neighbourhood of the second order domain of the destabilizing transition.

These observations are discussed with the help of a 2D Ginzburg–Landau model, derived from symmetry arguments [8]. The analytical and numerical analyses of the derived G–L equation are in good qualitative agreement with the character of the fingers growth and the thermodynamical analysis described in [7], with our experimental observations concerning static patterns, and with the out of equilibrium phenomena involving the formation of Archimedian spirals.

We acknowledge the contribution of T. Frisch to the theoretical part of this work and the I.N.R.I.A., Sophia Antipolis, where the numerical simulations were performed.

References

[1] COULLET, P., LEGA, J., HOUCHMANZADEH, B., and LAJZEROWICZ, J., 1990, *Phys. Rev. Lett.*, **65,** 1352. COULLET, P., LEGA, J., and POMEAU, Y., 1991, *Europhysics Lett.*, **15,** 221.

[2] DEVREOTES, P. N., 1983, *Adv. Cycl. nucl. Res.*, **15,** 55.

[3] VIDAL, C., and PACAULT, A., 1981, *Nonlinear Phenomena in Chemical Dynamics* (Springer-Verlag).

[4] GILLI, J. M., MORABITO, M., and FRISCH, T., 1994, *J. Phys. II France*, **4,** 319. FRISCH, T., RICA, S., COULLET P., and GILLI, J. M., 1994, *Phys. Rev. Lett.*, **72,** 1471.

[5] PRESS, M. J., and ARROT, A. S., 1976, *J. Phys., France*, **37,** 387.

[6] RIBIERE, P., and OSWALD, P., 1990, *J. Phys., France*, **51,** 1703.

[7] (a) RIBIERE, P., 1992, Ph.D thesis, Université C. Bernard, Lyon 1, France. (b) RIBIERE, P., PIRKL, S., and OSWALD, P., 1991, *Phys. Rev.* A, **44,** 8198.

[8] GIL, L., GILLI, J. M., and FRISCH, T., 1993, *Phys. Rev.* E, **48,** R4199.

[9] GILLI, J. M., and KAMAYE, M., 1992, *Liq. Crystals*, **12,** 545. GILLI, J. M., KAMAYE, M., and SIXOU, P., 1990, *J. Phys. France, Suppl.*, **51,** C7-183.

[10] GILLI, J. M., and KAMAYE, M., 1992, *Liq. Crystals*, **11,** 569.

[11] PIRKL, S., RIBIERE, P., and OSWALD, P., 1993, *Liq. Crystals*, **13,** 413.

[12] HAAS, W. E. K., and ADAMS, J. E., 1974, *Appl. Phys. Lett.*, **25,** 263. KAWACHI, M., KOGURE, O., and KATO, Y., 1974, *Jap. J. appl. Phys.*, **13,** 1457.

[13] GILLI, J. M., and KAMAYE, M., 1992, *Liq. Crystals*, **11,** 791.

[14] HINOV, H. P., and KUKLEVA, E., 1984, *Molec. Crystals liq. Crystals*, **109,** 203.